NEURAL REGENERATION RESEARCH
October 2017, Volume 12, Issue 10
www.nrronline.org

RESEARCH ARTICLE

Central projections and connections of lumbar primary afferent fibers in adult rats: effectively revealed using Texas red-dextran amine tracing

Shi-de Lin[1, 2, #], **Tao Tang**[1, #], **Ting-bao Zhao**[2], **Shao-jun Liu**[1, *]
1 State Key Laboratory of Proteomics, Department of Neurobiology, Beijing Institute of Basic Medical Sciences, Beijing, China
2 Department of Spinal Cord Injury, the General Hospital of Jinan Military Command, Jinan, Shandong Province, China

How to cite this article: *Lin SD, Tang T, Zhao TB, Liu SJ (2017) Central projections and connections of lumbar primary afferent fibers in adult rats: effectively revealed using Texas red-dextran amine tracing. Neural Regen Res 12(10):1695-1702.*
Funding: *This study was supported by the Medical Sciences Foundation of China, No. 14CXZ007.*

Graphical Abstract

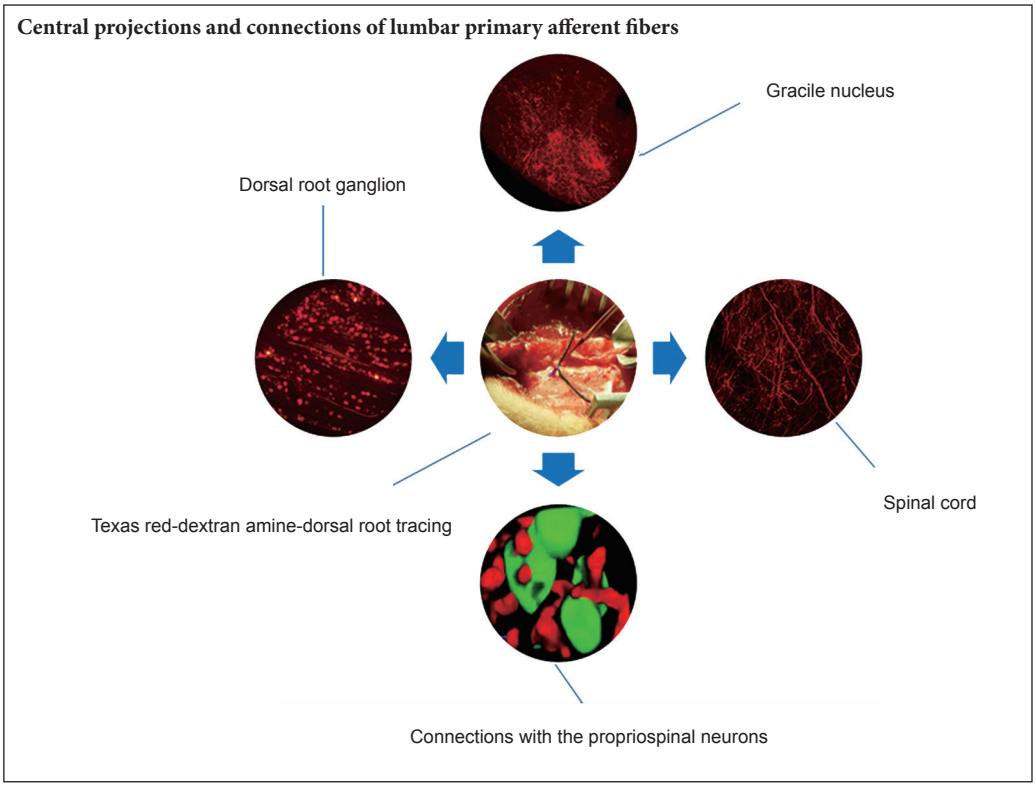

***Correspondence to:**
Shao-jun Liu, Ph.D., liusj@bmi.ac.cn.

#These authors contributed equally to this study.

orcid:
0000-0001-7318-7628 (Shao-jun Liu)

doi: *10.4103/1673-5374.217371*

Accepted: *2017-07-04*

Abstract

Signals from lumbar primary afferent fibers are important for modulating locomotion of the hind-limbs. However, silver impregnation techniques, autoradiography, wheat germ agglutinin-horseradish peroxidase and cholera toxin B subunit-horseradish peroxidase cannot image the central projections and connections of the dorsal root in detail. Thus, we injected 3-kDa Texas red-dextran amine into the proximal trunks of L_4 dorsal roots in adult rats. Confocal microscopy results revealed that numerous labeled arborizations and varicosities extended to the dorsal horn from T_{12}–S_4, to Clarke's column from T_{10}–L_2, and to the ventral horn from L_{1-5}. The labeled varicosities at the L_4 cord level were very dense, particularly in laminae I–III, and the density decreased gradually in more rostral and caudal segments. In addition, they were predominately distributed in laminae I–IV, moderately in laminae V–VII and sparsely in laminae VIII–X. Furthermore, direct contacts of lumbar afferent fibers with propriospinal neurons were widespread in gray matter. In conclusion, the projection and connection patterns of L_4 afferents were illustrated in detail by Texas red-dextran amine-dorsal root tracing.

Key Words: *nerve regeneration; spinal cord injury; dorsal root; central projection; connection; Texas red-dextran amine; neural regeneration*

Introduction

Spinal cord injury can be disastrous, often leading to lifelong disability and seriously impacting patients' physical and mental health, and the outcomes of current treatments are still poor (Schonherr et al., 2000; Dunn et al., 2009; Mulcahey et al., 2010; Byrnes et al., 2012; Tian et al., 2014). For more than 16 years, we have been attempting to repair spinal cord transection by intercostal nerve-lumber dorsal root anastomosis, obtaining a number of promising outcomes (unpublished). The vertebrate central pattern generators (CPGs) located in the spinal cord form the neuroanatomical basis of our novel treatment strategy for spinal cord injury. CPGs are comprised of afferent nerves, interneuron units and efferent nerves. The interactions between the elements of CPGs cause neural oscillations and rhythmic impulses, and the interplay among CPGs harmonically generates different modes of locomotion, such as swimming, walking and running (McCrea and Rybak, 2008; Rybak et al., 2015). Although there have been significant advances in CPG research, the precise neural mechanisms underlying coordinative locomotion remain unclear. Signals from lumbar primary afferents are important for locomotion modulation of the hind-limbs (Menard et al., 2002; Sirois et al., 2013), and their projection scopes and synaptic connections with the propriospinal neurons in the spinal cord may be beneficial for elucidating the mechanisms of CPGs. However, quantitative analysis of varicosities from the dorsal root in the spinal cord has not previously been reported. In the current study, we applied 3-kDa Texas red-dextran amine (TRDA) for fine labeling of nerve fibers and varicosities (Fritzsch, 1993), and obtained images of the whole central projections and connections of lumbar afferent fibers by directly injecting TRDA into the proximal trunks of the L_4 dorsal root.

Materials and Methods

Animals

A total of 20 adult female specific-pathogen-free Sprague-Dawley rats (weighing 260–300 g, aged 7–8 weeks), supplied by the Laboratory Animal Center of the Academy of Military Medical Sciences (SCXK-(Army)-2012-004), were housed in temperature- and humidity-controlled rooms (25 ± 1°C; 45 ± 5%) with a 12-hour light/dark photoperiod. Animals were housed in groups of three rats per cage, and given free access to chow and water during the experiment. All experimental procedures were carried out in accordance with the EU Directive 2010/63/EU for animal experiments, and were approved by the Beijing Institute of Basic Medical Sciences in China.

Labeling procedures

Animals were anesthetized with 1.0% sodium pentobarbital solution (50 mg/kg body weight) *via* intraperitoneal injection, and the body temperature was maintained using a heating pad during surgery. After laminectomy, the right L_4 dorsal roots were exposed, and approximately 0.46 μL 10% TRDA (catalog No. D3328, lot No.: 1540675, Molecular Probes, Eugene, OR, USA) dissolved in ddH_2O was slowly injected into the trunks, 10 mm proximal to L_4 dorsal root ganglions (DRGs) using glass micropipettes (OD 30–40 μm) with NANOJECTII (Drummond Scientific Company, Broomall, PA, USA). The pipettes were kept in place for a further 5 minutes, and the injection sites (**Additional Figure 1**) were dabbed with cotton swabs then flushed three times with sterile saline solution to avoid contamination. Finally, the wounds were closed with layered sutures. In another group, 10% TRDA with the same volume was directly injected into the right L_4 DRGs, with 2–3 injection sites for comparing the labeling efficiencies between two injection methods (**Table 1**).

Table 1 Number of animals examined using dorsal root ganglion tracing and dorsal root tracing methods

Survival time (day)	Dorsal root ganglion tracing	Dorsal root tracing
3		3
7		2+1*
10	3	3+1*
14	3	3+1*

*The spinal cord was cut horizontally

Tissue processing and detection

At 3–14 days postoperatively, animals were deeply re-anesthetized with an overdose of sodium pentobarbital, then transcardially perfused with 200 mL 0.9% sodium chloride solution followed by 500 mL specific buffer of 4% paraformaldehyde. The brain stems with gracile nucleus, T_{10}–S_4 segments of spinal cords, and $L_{3–5}$ DRGs of both sides were removed, cryoprotected in phosphate buffered saline (PBS, pH 7.4) containing 20% sucrose, and stored at 4°C overnight.

All DRGs were cut into 20-μm longitudinal sections using a cryostat microtome (0001EU, Seward, West Sussex, UK), and digital images were captured with a fluorescence microscope (Olympus BX50, Shinjuku, Tokyo, Japan) using DP2-BSW software (Olympus) with the parameters 4 × air (numerical aperture [NA] = 0.13). Six images of the right L_4 DRG of each rat were randomly selected, and the labeled and unlabeled neurons in the same image were manually identified and counted using Fiji software, downloaded from http://fiji.sc/Downloads#Fiji. The uptake ratio (labeling ratio) of TRDA was determined by dividing the quantity of the labeled neurons by the total neurons in the same section. Simultaneously, more than 150 TRDA-labeled sensory neurons in DRGs were randomly selected, and their diameters were measured using Fiji software.

All of the gracile nuclei and spinal cords were cut into 40-μm thick coronal sections, except for three cases that were cut into horizontal sections (**Table 1**), and fluorescence photomicrographs were captured with a confocal microscope

(TIE-A1, Nikon, Otawara, Tochigi, Japan) using NIS-Elements 4.40 software (Nikon). The diameters of 150 axons and varicosities in spinal cords were measured using Volocity 6.0.1 software (PerkinElmer, Fremont, CA, USA). To more precisely illustrate the distribution patterns of varicosities in the spinal cord, 3–6 sections of T_{12}–L_6 cord levels were randomly picked up, and large scopes (4,711 pixels × 7,476 pixels, 10% overlay) with Z-stacks (0.5 μm/step × 10–30 steps) were captured. The densities of varicosities in different laminae were calculated using the 3D objector counter in Fiji software v2.0. The value of the size filter was 10–100 pixels, set after more than 100 varicosities were manually measured, and the intensity threshold was finely adjusted according to the brightness of the images.

In addition, some coronal sections of L_4 segments were selected for immunofluorescence to examine the relationships between the primary afferents and the propriospinal neurons. The sections were blocked and pre-permeated with 1% bovine serum albumin containing 0.3% Triton X-100 for 30 minutes at room temperature, then incubated overnight at 4°C with the primary antibody of mouse anti-neuron specific nuclear protein (anti-NeuN, 1:1,000; catalog No. ab104224, lot No. GR138829, monoclonal; Abcam, Cambridge, MA, USA), which was tested for specificity using western blot assay according to the datasheet provided by the supplier. The quality of staining obtained in the present study was confirmed by comparison with the images from previous studies (Kaur et al., 2014; Li et al., 2014), in which the same antibody was applied. After incubation with FITC-conjugated goat anti-mouse IgG (1:200; catalog No. EM35120-01, lot No. 3001; Emarbio Science & Technology Co., Ltd., Beijing, China) for 2 hours at room temperature, all sections were mounted on poly-lysine pre-coated slides and coverslipped` with mounting medium (Fluoromount, catalog No. F4680, lot No. SLBN9322V; Sigma-Aldrich). All slides were kept in the dark at 4°C till observation, and digital images were acquired with TIE-A1 confocal microscopy (Nikon) using NIS-Elements 4.40 software (Nikon). TRDA was visualized at 561 nm (Solid Laser561/50w Display/DE), and FITC-conjugated secondary antibody was excited at 488 nm (Multi Ar Laser65mW/US). All images were scanned at a resolution of 1,024 × 1,024 pixels using the following parameters: 10 × air (NA = 0.45, pinhole = 19.2 μm), 20 × air (NA = 0.75, pinhole = 23.0 μm), 40 × air (NA = 0.95, pinhole = 38.3 μm) and 60 × oil (NA = 1.4, pinhole = 39.6 μm). Z-stacks through the depth of the sections were acquired, and the intervals ranged from 0.2 μm to 0.5 μm depending on the detection aims.

Statistical analysis

All measurements were performed by the same observer, and data were calculated as the mean ± SD. Efficiency analysis was conducted using *t*-tests or one-way analysis of variance followed by Dunnett's T3 adjustment for multiple comparisons with the SPSS 21.0 software package (IBM, Armonk, NY, USA). A value of $P < 0.05$ was considered statistically significant.

Results

Labeling efficiency of two injection methods

When TRDA was injected into L_4 DRGs, a high amount of tracer was present in the area surrounding the neurons in DRGs, but only a small amount was taken up (**Figure 1A**). The uptake ratios were 11.81 ± 3.94% and 10.86 ± 3.38% at 10 and 14 days post-operation, respectively. These ratios were not correlated with the survival time ($P > 0.05$; **Figure 2A** and **C**). To improve labeling efficiency, we directly injected TRDA into the trunks of L_4 dorsal root, where they were taken up and retrogradely transported to the cell bodies in DRGs (**Figure 1B**). The ratios of labeled neurons were 47.09 ± 5.68%, 46.23 ± 8.62% and 48.34 ± 10.44% at 3, 7 and 10 days post-operation, respectively, and there were no significant differences between them ($P > 0.05$). When the survival time was extended to 14 days, the labeling ratio increased to 65.58 ± 5.49%, which was much higher than that at any other time points (**Figure 1C**; $P < 0.01$). Furthermore, the labeling ratios of dorsal root tracing were much higher than those of DRG tracing at 10 and 14 days postoperatively ($P < 0.01$; **Figures 1D**, **2B**, **2D**–**F**).

In addition, TRDA labeled the small diameter neurons (≤ 30 μm) as well as the large ones (> 30 μm). The diameters of labeled neurons ranged from 5.09 μm to 42.53 μm. Small neurons accounted for 90.7% of labeled cells. The diameters of labeled axons in the spinal cord ranged from 0.31 μm to 8.4 μm, while the diameters of varicosities ranged from 1.32 μm to 16.97 μm. None of the neurons in bilateral L_3, L_5 and contralateral L_4 DRGs were labeled.

Central projections of L_4 primary afferents

After tracers were injected into L_4 dorsal roots, they were uptaken and anterogradely transported to the axon terminals in the spinal cord and gracile nucleus. At 3 days postoperatively, only a small number of TRDA-labeled terminals were ipsilaterally distributed in the dorsal funiculus and laminae I–V at L_4 segment. At 7, 10 and 14 days postoperatively, the projection scopes were extended to the T_{10}–S_4 cord levels, and the density and intensity of labeled varicosities increased with the extension of survival time.

The horizontal sections of spinal cord revealed that a large number of labeled primary afferent fibers ascended in the posterior funiculus and projected to the brain stem, while a small quantity of them descended to the sacral cords (**Additional Figure 2**). A large number of labeled arborizations and varicosities were widely distributed in different laminae of ipsilateral spinal cords, which longitudinally extended in the lateral part of the superficial dorsal horn (laminae I–III; **Figure 3B** and **C**), while transversely extending in the deep dorsal horn (laminae V–VII; **Figure 3E** and **F**). Furthermore, a small number of cross-projecting nerve fibers and varicosities were also observed in the

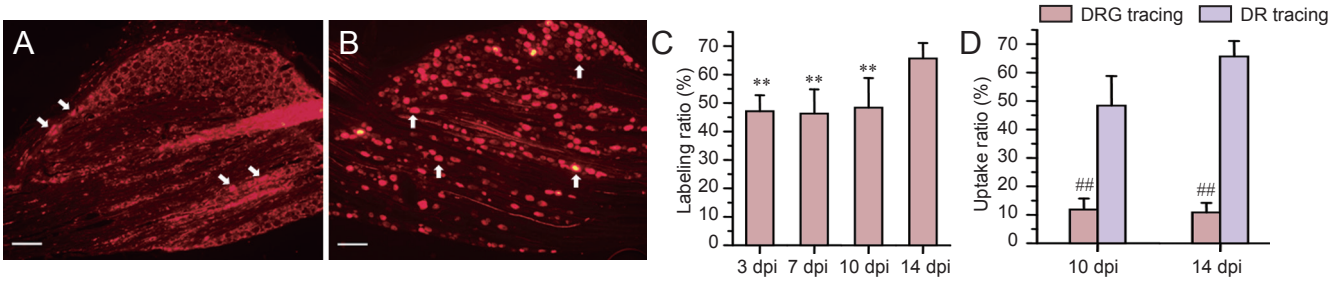

Figure 1 Labeling efficiency of dorsal root ganglion (DRG) tracing and dorsal root (DR) tracing.
(A) When Texas red-dextran amine (TRDA) was injected into L_4 DRG, a large amount of tracer was present in the area surrounding the neurons in DRG but only a small proportion (approximately 10%) of cells were labeled. (B) However, most (> 50%) of the neurons in DRG were labeled when TRDA was injected into the trunk of the L_4 DR. Scale bars: 200 μm. Arrows: Neurons labeled by TRDA. (C) The labeling ratios were not significantly different at 3, 7 and 10 days after DR tracing ($P > 0.05$), and they were all lower compared with 14 days after DR tracing (**$P < 0.01$, *vs.* 14 days after DR tracing). (D) Furthermore, the uptake ratios of DR tracing were much higher than those of DRG tracing at 10 and 14 days postoperatively (##$P < 0.01$, *vs.* DR tracing). Data are presented as the mean ± SD. Efficiency analysis was conducted using *t*-tests (D) or one-way analysis of variance followed by Dunnett's T3 adjustment for multiple comparisons (C). dpi: Days post-injection.

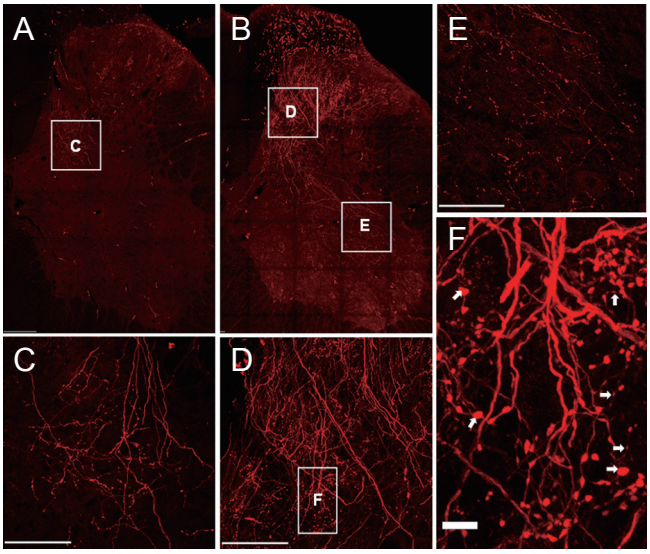

Figure 2 Transverse sections through the L_4 cord level at 10 days after TRDA injection.
Large scopes were captured using Nikon TIE-A1 confocal microscopy with 10% overlay (A and B). Modicum axon arborizations and varicosities were labeled after DRG tracing (C, 0.5 μm/step × 25 steps), while many labeled fibers and varicosities were distributed in the dorsal and ventral horns of the L_4 segment after DR tracing (D and E, 0.5 μm/step × 22–24 steps). Higher magnification of the boxed area in D showed that TRDA filled the small as well as large axons and varicosities (F, 0.2 μm/step × 87 steps, arrow: varicosity labeled by TRDA). Scale bars: 250 μm in A and B, 100 μm in C–E, 10 μm in F (0.5 μm/step × 25 steps: Z-stacks through the depth of the sections, with an interval of 0.5 μm). TRDA: Texas red-dextran amine.

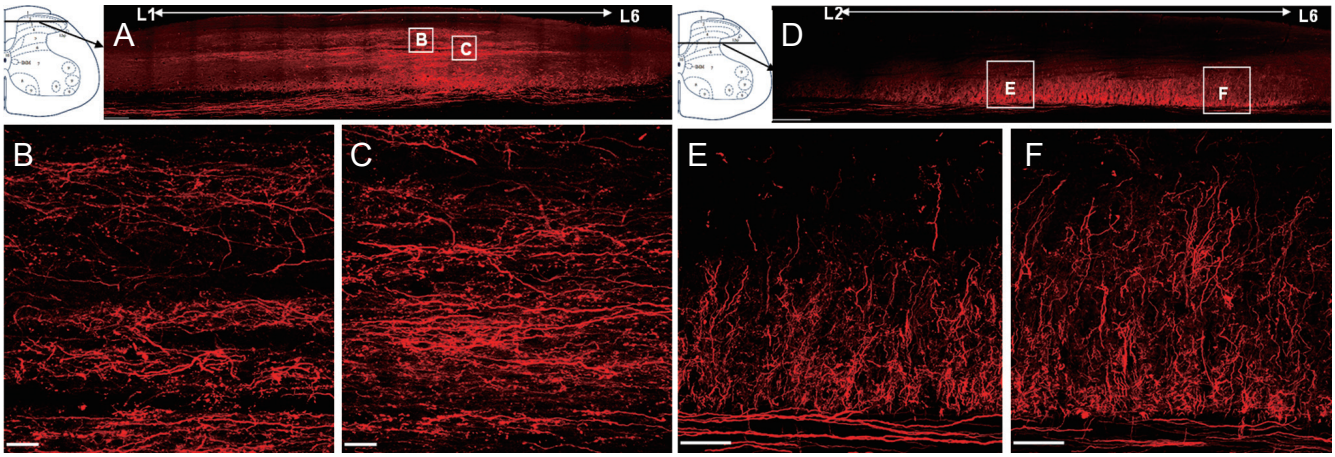

Figure 3 Photomicrographs of horizontal section of lumbar spinal cord at 10 days after dorsal root tracing.
(A, D) Large scopes were captured using Nikon TIE-A1 confocal microscopy with 5% overlay. A large number of labeled nerve fibers and varicosities were widely distributed in ipsilateral lumbar cord at 10 days after dorsal root tracing, and extended longitudinally in the lateral part of the superficial dorsal horn (B and C 0.5 μm/step × 24–25 steps), while extending transversely in the deep dorsal horn (E and F, 0.5 μm/step × 34 steps). (B, C, E, F) Magnification of the box area in A and D. Scale bars: 500 μm in A and D, 100 μm in B, C, E and F.

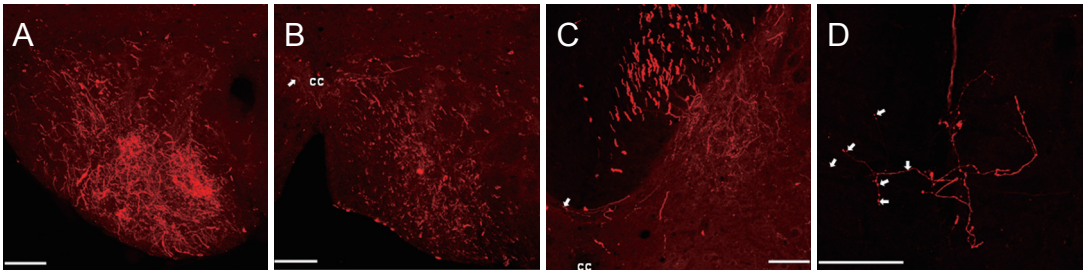

Figure 4 Long distance projections and cross projections of L_4 afferent fibers at 14 days after dorsal root tracing.
(A, B) A large number of labeled arborizations and varicosities were ipsilaterally distributed throughout the whole gracile nucleus (A, 0.5 μm/step × 50 steps) and a small number cross-projected to the contralateral gracile nucleus (arrow in B, 0.5 μm/step × 31 steps) at 14 days after dorsal root tracing. (C, D) In addition, a small number of cross-projecting nerve fibers and varicosities were also observed at the commissural regions of lamina X (arrow in C, transverse section, 0.2 μm/step × 79 steps, and arrows in D, horizontal section, 0.5 μm/step × 22 steps). Scale bars: 100 μm. cc: Central canal.

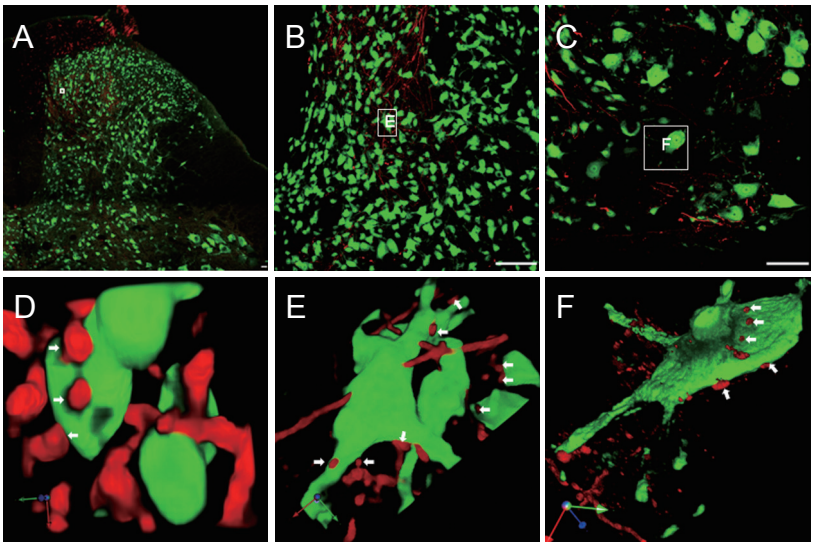

Figure 5 Relationships of the primary afferent fibers with the propriospinal neurons in L_4 gray matter.
After dorsal root tracing, abundant arborizations and varicosities labeled by Texas red-dextran amine (red) were found in the gray matter of the L_4 cord level, and some were closely connected with the NeuN positive neurons (green), forming direct contacts between them (arrows in D–F, 3D opacity mode of the boxed area in A–C, 0.2 μm/step × 65–107 steps). Moreover, these contacts were widespread in the gray matter, and predominantly localized in laminae III–V of the ipsilateral dorsal horn. (A) Laminae I–VI; (B) laminae III–V; (C) laminae VIII and IX. Scale bars: 100 μm in A–C.

Table 2 Density (numbers/mm^3) of varicosities in the spinal cord of rats

Lamina	T_{12}	T_{13}	L_1	L_2
I–III*	34,737±16,774	47,050±9,150	71,005±31,845	218,062±37,324
IV	52,481±27,128	32,839±6,137	62,612±28,844	226,258±69,036
V	26,099±13,556	28,978±14,584	27,019±6,182	49,776±13,544
VI	–	–	–	–
VII	23,842±4,917	33,930±18,935	30,790±12,141	39,245±33,176
VIII	–	–	38,338±27,493	35,472±7,146
IX	–	–	13,815±7,640	20,131±2,389
X	–	–	47,096±23,452	68,488±33,804
Clarke's column	137,879±20,102	294,389±164,034	381,616±81,775	715,336±206,338
Intermediomedial cell column	–	–	57,200±11,766	70,290±76,659

Lamina	L_3	L_4	L_5	L_6
I–III*	715,085±589,552	2,466,678±1,030,612	253,361±66,537	139,624±26,126
IV	738,459±692,680	2,345,097±799,718	195,345±37,503	100,682±47,409
V	374,226±251,249	1,220,612±980,612	51,523±21,623	43,009±11,772
VI	263,819±239,042	776,153±640,360	31,936±11,527	35,392±8,369
VII	44,817±41,258	560,620±374,254	14,789±3,374	18,628±3,019
VIII	46,628±34,274	412,913±370,210	16,579±2,559	7,437±1,429
IX	36,779±17,208	254,457±146,312	22,817±14,117	9,569±2,230
X	60,539±45,986	375,844±217,144	40,106±24,565	15,661±11,450
Clarke's column	–	–	–	–
Intermediomedial cell column	74,164±72,808	580,748±328,904	40,053±54,586	71,754±31,333

*Densities of varicosities in laminae I–III were very similar, so they were calculated together.

dorsal commissural region of lamina X in the T_{13} segment (arrows in **Figure 4D**).

In the coronal sections, a large quantity of labeled nerve fibers and varicosities were ipsilaterally localized in T_{10}–S_4 segments, which extended to Clarke's column at T_{10} and T_{11}, to laminae I–VII and Clarke's column at T_{12} and T_{13}, to laminae I–VII including Clarke's column and intermediomedial cell column at L_1 and L_2, to all laminae including intermediomedial cell column and Lissauer's tract from $L_{3–5}$, to laminae I–VII, X and intermediomedial cell column at L_6, and to laminae IV–VI from $S_{1–4}$ cord levels (**Additional Figure 3**). **Table 2** shows the rostrocaudal distributions of labeled varicosities in spinal cord, which was very dense at the L_4 cord level, particularly in laminae I–III (2,466,678/mm^3), and decreased gradually in more rostral and caudal segments. The labeled varicosities were predominately distributed in laminae I–IV, moderately in laminae V–VII and sparsely in laminae VIII–X in the lumbar cords. Moreover, many of the labeled varicosities were distributed in Clarke's column from T_{10} to L_2 segments (137,879–715,336/mm^3).

None of the nerve terminals in the gracile nucleus were labeled at 3–10 days postoperatively. However, a large number of labeled arborizations and varicosities ipsilaterally extended throughout the whole gracile nucleus (**Figure 4A** and **B**) in three rats (but were sparse in one rat) when the survival time was extended to 14 days. Moreover, a small number of cross-projections from the L_4 dorsal root to the contralateral gracile nuclei and spinal cord were also observed (arrows in **Figure 4B** and **C**).

Relationships of primary afferent fibers with propriospinal neurons in gray matter

After double fluorescence photomicrographs of the coronal sections of the L_4 segment were captured, close appositions between the TRDA-labeled varicosities and FITC-stained somata as well as dendrites of the propriospinal neurons were identified in a 3D opacity mode using Volocity 6.0.1 software. Appositions were regarded as physical contacts when no gaps were observed. **Figure 5** shows that numerous labeled arborizations and varicosities originating from the L_4 dorsal root were located in spinal cord, and some of them were strongly connected with NeuN-positive neurons forming direct contacts between them. These contacts were widespread in the gray matter, and predominately localized in laminae III–V of ipsilateral dorsal horn (**Figure 5A**, **B**, **D** and **E**), and were sparsely distributed in laminae VIII and IX of the ipsilateral ventral horn (**Figure 5C** and **F**), where motor neurons were located.

Discussion

Dorsal root tracing performs better than DRG tracing in terms of labeling efficiency

The results revealed that 3-kDa TRDA was an efficient anterograde and retrograde tracer in the present study, achieving sensitive and fine anterograde labeling of entire axons, arborizations and varicosities in the spinal cord and gracile nucleus, and retrograde labeling of cell bodies in the DRG. When TRDA was applied to the DRG, only approximately 10% of sensory neurons and a small number of terminals in the spinal cord were labeled. This low proportion may be related to the nonhomogeneous distributions of the injected tracers, and/or injury of the neurons in DRG. However, when TRDA was directly injected into the dorsal root, about 50% of neurons in DRG and a large quantity of varicosities distributed from T_{10} to S_4 cord levels were labeled, suggesting that the labeling efficiency of dorsal root tracing was much higher than that of DRG tracing, possibly because TRDA could be taken up by damaged as well as intact axons in the injection site. In addition, the labeling efficiency of dorsal root tracing was much higher compared with biotin-dextran amine tracing described in a previous study (Novikov, 2001). Although viral tracing techniques appear to be superior to classic tracing approaches (Novikov, 2001; Mason et al., 2010), which can also transsynaptically transfer and delineate output connectivity with third-order neurons (Zampieri et al., 2014), the required laboratory conditions and experimental operations are demanding. Dextran amines are safe, non-toxic, efficient and easy-to-use tracers, which cannot diffuse out of the cells, even when anterograde tracing is combined with immunological or histochemical procedures (Schmued et al., 1990; Vercelli et al., 2000). Therefore, dorsal root tracing using TRDA may provide an appropriate choice for labeling of the primary afferent fibers.

Central projections of the single dorsal root are extensive and complex

The central projections of primary afferent fibers have been traced using Golgi methodologies (Hamano et al., 1978), silver impregnation techniques (Kusuma and ten Donkelaar, 1980), autoradiography (Snyder, 1982), horseradish peroxidase (HRP) (Light and Perl, 1977; Proshansky and David Egger, 1977; Mesulam and Brushart, 1979), cholera toxin B subunit-HRP (CB-HRP) (Robertson and Grant, 1985; Rivero-Melian and Grant, 1990), wheat germ agglutinin-HRP (WGA-HRP) (Robertson and Grant, 1985) and other tracers (Novikov, 2001) (viral vectors were not discussed in this manuscript). However, the results have not been entirely consistent, and most of these previous studies have concentrated solely on the restricted medullary regions receiving afferent fibers from target tissues, organs or the nerves they govern (Mesulam and Brushart, 1979; Cervero et al., 1984; Pfister and Zenker, 1984; Robertson and Grant, 1985; Molander and Grant, 1987; LaMotte et al., 1991; Novikov, 2001), and the whole central projections and connections of single dorsal roots has not previously been reported.

When projections of the sciatic nerve, which is formed mainly by the $L_{4–5}$ DRGs (Rivero-Melian and Grant, 1990), were traced using CB-HRP or in combination with WGA-

HRP, afferents were found to extend to the dorsal horn from L_1–S_1, to Clarke's column from T_8–L_1, to the ventral horn from L_{2-5}, and throughout the medial and dorsal region of the gracile nucleus (LaMotte et al., 1991). Another report revealed more extensive distributions of L_4 primary afferent fibers in spinal cord after L_4 DRG tracing with CB-HRP (Rivero-Melian and Grant, 1990). However, the marginal zone and the substantia gelatinosa were devoid of labeling (Robertson and Grant, 1985; Rivero-Melian and Grant, 1990). In the present study, numerous labeled arborizations and varicosities extended to the dorsal horn from T_{12}–S_4, to Clarke's column from T_{10}–L_2, to the ventral horn from L_{1-5}, and the labeled varicosities were predominately distributed in laminae I–IV, moderately in laminae V–VII and sparsely in laminae VIII–X according to quantitative analysis. Moreover, the marginal zone and substantia gelatinosa showed very strong labeling in L_{3-5} segments because TRDA labeled small as well as large diameter axons and varicosities, unlike CB-HRP or WGA-HRP tracing (Robertson and Grant, 1985). Furthermore, the TRDA-labeled nerve fibers interweaved in the lumbar cords, which longitudinally extended in the lateral of superficial dorsal horn, as suggested by Light and Perl (Light and Perl, 1977), while transversely extending in the deep dorsal horn. Thus, the elaborated distributions of the L_4 dorsal root were illustrated more precisely than in earlier studies.

Relationships between primary afferent fibers and propriospinal neurons

The phenotype of synapses that make up the neural circuits of specific neural systems can be elucidated when anterograde tracing is combined with immunocytochemistry technologies (Raju and Smith, 2006). Moreover, the detailed and precise characterization of the cell's morphology and their contact with other neurons or fibers is simplified with the development of three-dimensional reconstruction techniques using a confocal laser scanning microscope (Wallen et al., 1988). In the current research, primary antibody of NeuN, which is a sensitive and specific nuclear protein localizing in the nuclei and perinuclear cytoplasm of most of the neurons in the central nervous system (Mullen et al., 1992; Guo et al., 2015; Gusel'nikova and Korzhevskiy, 2015), was applied to illustrate the propriospinal neurons in gray matter, and their anatomic connections with primary afferent fibers from L_4 dorsal root were investigated using a 3D reconstruction technique. Although it is impossible to identify the synaptic connections at the light microscopic level, **Figure 5** shows that the terminal-like labeling was strongly relations to the stained neurons, indicating possible synaptic relationships between them. It is generally accepted that the roles of propriospinal neurons are diverse, according to their laminar distributions and connections (Harrison et al., 1986; Kato et al., 2009; Antal et al., 2016). The present study revealed that the contacts of the primary afferent fibers with the propriospinal neurons were widespread in gray matter. Furthermore, some of them contacted the motor neurons in the ventral horn, suggesting that signals from primary afferent fibers might take part in diverse neural circuits, such as CPGs, in the spinal cord. This finding may be useful for furthering our understanding of new strategies for repairing spinal cord transection by intercostal nerve-lumbar dorsal root anastomosis. In future, different neuronal markers should be applied to further elucidate the roles of primary afferent fibers in diverse neural circuits in the spinal cord.

Conclusions

The projection and connection patterns of lumbar primary afferent fibers were illustrated in detail by injecting TRDA into the L_4 dorsal root, and a large number of labeled nerve fibers and varicosities were extensively distributed in the spinal cord, and widely contacted propriospinal neurons.

Acknowledgments: *The authors are grateful to Kai Wang (National Center of Biomedical Analysis, China), Chao Yuan (Center of Cognition and Brain Science, Institute of Basic Medical Science, China) and Xin Xu (National Center of Biomedical Analysis, China) for their kind assistances with confocal microscopy.*

Author contributions: *All authors had full access to all the data in the study and took responsibility for the integrity of the data and the accuracy of the data analysis. Study concept and design: SJL and SDL. Acquisition of data, drafting of the manuscript: SDL. Analysis and interpretation of data: SDL and TT. Critical revision of the manuscript for important intellectual content: TT. Statistical analysis: TBZ. Obtained funding: SJL. Administrative, technical, material support, and study supervision: SJL. All author approved the final version of this paper.*

Conflicts of interest: *None declared.*

Research ethics: *The study protocol was approved by the Ethics Committee of Beijing Institute of Basic Medical Sciences, China. The experimental procedure followed the National Institutes of Health Guide for the Care and Use of Laboratory Animals (NIH Publications No. 8023, revised 1978).*

Data sharing statement: *Datasets analyzed during the current study are available from the corresponding author on reasonable request.*

Plagiarism check: *Checked twice by iThenticate.*

Peer review: *Externally peer reviewed.*

Open peer reviewers: *Masaaki Hori, Juntendo University, Japan; Mitsuhiro Enomoto, Tokyo Medical and Dental University, Japan.*

Additional file

Additional Figure 1: DR tracing technique.

Additional Figure 2: Horizontal section of posterior funiculus of spinal cord after L_4 DR tracing (A), Higher magnification of the boxed area in A (B).

Additional Figure 3: Distributions of TRDA in gracile nucleus (A), T_{10}–S_4 (B–O) segments of spinal cord and sciatic nerve (P) after L_4 DR tracing. Higher magnification of the boxed areas in L–O (Q–T).

References

Antal Z, Luz LL, Safronov BV, Antal M, Szücs P (2016) Neurons in the lateral part of the lumbar spinal cord show distinct novel axon trajectories and are excited by short propriospinal ascending inputs. Brain Struct Funct 221:2343-2360.

Byrnes M, Beilby J, Ray P, McLennan R, Ker J, Schug S (2012) Patient-focused goal planning process and outcome after spinal cord injury rehabilitation: quantitative and qualitative audit. Clin Rehabil 26:1141-1149.

Cervero F, Connell LA, Lawson SN (1984) Somatic and visceral primary afferents in the lower thoracic dorsal root ganglia of the cat. The Journal of comparative neurology 228:422-431.
Dunn J, Sinnott KA, Nunnerley J, Scheuringer M (2009) Utilisation of patient perspective to validate clinical measures of outcome following spinal cord injury. J Disabil Rehabil 31:967-975.
Fritzsch B (1993) Fast axonal diffusion of 3000 molecular weight dextran amines. Neurosci Methods 50:95-103.
Guo JH, Ma W, Yang JW, Gao Y, Liang Z, Liu J, Wang DY, Luo T, Cheng JR, Li LY (2015) Expression pattern of NeuN and GFAP during human fetal spinal cord development. Childs Nervous Syst 31:863-872.
Gusel'nikova VV, Korzhevskiy DE (2015) NeuN As a neuronal nuclear antigen and neuron differentiation marker. Acta Naturae 7:42-47.
Hamano K, Mannen H, Ishizuka N (1978) Reconstruction of trajectory of primary afferent collaterals in the dorsal horn of the cat spinal cord, using Golgi-stained serial sections. J Comp Neurol 181:1-15.
Harrison PJ, Jankowska E, Zytnicki D (1986) Lamina VIII interneurones interposed in crossed reflex pathways in the cat. J Physiol 371:147-166.
Kato G, Kawasaki Y, Koga K, Uta D, Kosugi M, Yasaka T, Yoshimura M, Ji RR, Strassman AM (2009) Organization of intralaminar and translaminar neuronal connectivity in the superficial spinal dorsal horn. J Neuroscience 29:5088-5099.
Kaur P, Karolina DS, Sepramaniam S, Armugam A, Jeyaseelan K (2014) Expression profiling of RNA transcripts during neuronal maturation and ischemic injury. PloS One 9:e103525.
Kusuma A, ten Donkelaar HJ (1980) Dorsal root projections in various types of reptiles. Brain Behav Evol 17:291-309.
LaMotte CC, Kapadia SE, Shapiro CM (1991) Central projections of the sciatic, saphenous, median, and ulnar nerves of the rat demonstrated by transganglionic transport of choleragenoid-HRP (B-HRP) and wheat germ agglutinin-HRP (WGA-HRP). J Comp Neurol 311:546-562.
Li XQ, Cao XZ, Wang J, Fang B, Tan WF, Ma H (2014) Sevoflurane preconditioning ameliorates neuronal deficits by inhibiting microglial MMP-9 expression after spinal cord ischemia/reperfusion in rats. Mol Brain 7:69.
Light AR, Perl ER (1977) Differential termination of large-diameter and small-diameter primary afferent fibers in the spinal dorsal gray matter as indicated by labeling with horseradish peroxidase. Neurosci Lett 6:59-63.
Mason MR, Ehlert EM, Eggers R, Pool CW, Hermening S, Huseinovic A, Timmermans E, Blits B, Verhaagen J (2010) Comparison of AAV serotypes for gene delivery to dorsal root ganglion neurons. Mol Ther 18:715-724.
McCrea DA, Rybak IA (2008) Organization of mammalian locomotor rhythm and pattern generation. Brain Res Rev 57:134-146.
Menard A, Leblond H, Gossard JP (2002) Sensory integration in presynaptic inhibitory pathways during fictive locomotion in the cat. J Neurophysiol 88:163-171.
Mesulam MM, Brushart TM (1979) Transganglionic and anterograde transport of horseradish peroxidase across dorsal root ganglia: a tetramethylbenzidine method for tracing central sensory connections of muscles and peripheral nerves. Neuroscience 4:1107-1117.
Molander C, Grant G (1987) Spinal cord projections from hindlimb muscle nerves in the rat studied by transganglionic transport of horseradish peroxidase, wheat germ agglutinin conjugated horseradish peroxidase, or horseradish peroxidase with dimethylsulfoxide. J Comp Neurol 260:246-255.
Mulcahey MJ, DiGiovanni N, Calhoun C, Homko E, Riley A, Haley SM (2010) Children's and parents' perspectives about activity performance and participation after spinal cord injury: initial development of a patient-reported outcome measure. Am J Occup Ther 64:605-613.
Mullen RJ, Buck CR, Smith AM (1992) NeuN, a neuronal specific nuclear protein in vertebrates. Development 116:201-211.
Novikov LN (2001) Labeling of central projections of primary afferents in adult rats: a comparison between biotinylated dextran amine, neurobiotin and Phaseolus vulgaris-leucoagglutinin. J Neurosci Methods 112:145-154.
Pfister J, Zenker W (1984) The splenius capitis muscle of the rat, architecture and histochemistry, afferent and efferent innervation as compared with that of the quadriceps muscle. Anat Embryol (Berl) 169:79-89.
Proshansky E, David Egger M (1977) Staining of the dorsal root projection to the cat's dorsal horn by anterograde movement of horseradish peroxidase. Neurosci Lett 5:103-110.
Raju DV, Smith Y (2006) Anterograde axonal tract tracing. Curr Protoc Neurosci Chapter 1:Unit 1.14.
Rivero-Melian C, Grant G (1990) Distribution of lumbar dorsal root fibers in the lower thoracic and lumbosacral spinal cord of the rat studied with choleragenoid horseradish peroxidase conjugate. J Comp Neurol 299:470-481.
Robertson B, Grant G (1985) A comparison between wheat germ agglutinin-and choleragenoid-horseradish peroxidase as anterogradely transported markers in central branches of primary sensory neurones in the rat with some observations in the cat. Neuroscience 14:895-905.
Rybak IA, Dougherty KJ, Shevtsova NA (2015) Organization of the mammalian locomotor CPG: review of computational model and circuit architectures based on genetically identified spinal interneurons(1,2,3). eNeuro 2.
Schmued L, Kyriakidis K, Heimer L (1990) In vivo anterograde and retrograde axonal transport of the fluorescent rhodamine-dextran-amine, Fluoro-Ruby, within the CNS. Brain Res 526:127-134.
Schonherr MC, Groothoff JW, Mulder GA, Eisma WH (2000) Prediction of functional outcome after spinal cord injury: a task for the rehabilitation team and the patient. Spinal Cord 38:185-191.
Sirois J, Frigon A, Gossard JP (2013) Independent control of presynaptic inhibition by reticulospinal and sensory inputs at rest and during rhythmic activities in the cat. J Neuroscience 33:8055-8067.
Snyder RL (1982) Light and electron microscopic autoradiographic study of the dorsal root projections to the cat dorsal horn. Neuroscience 7:1417-1437.
Tian F, Ni P, Mulcahey MJ, Hambleton RK, Tulsky D, Haley SM, Jette AM (2014) Tracking functional status across the spinal cord injury lifespan: linking pediatric and adult patient-reported outcome scores. Arch Phys Med Rehabil 95:2078-2085 e2015.
Vercelli A, Repici M, Garbossa D, Grimaldi A (2000) Recent techniques for tracing pathways in the central nervous system of developing and adult mammals. Brain Res Bull 51:11-28.
Wallen P, Carlsson K, Liljeborg A, Grillner S (1988) Three-dimensional reconstruction of neurons in the lamprey spinal cord in whole-mount, using a confocal laser scanning microscope. J Neurosc Methods 24:91-100.
Zampieri N, Jessell TM, Murray AJ (2014) Mapping sensory circuits by anterograde transsynaptic transfer of recombinant rabies virus. Neuron 81:766-778.

Copyedited by Knight B, Hindle A, Yu J, Li CH, Qiu Y, Song LP, Zhao M

Additional files

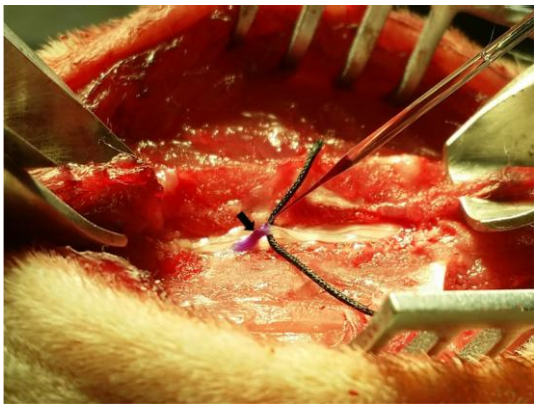

Additional figure 1: Dorsal root tracing technique

Arrow: Injection site

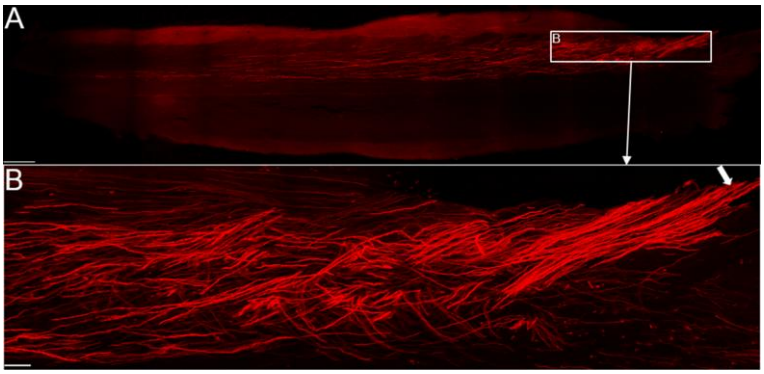

Additional figure 2: Horizontal section of posterior funiculus of spinal cord after L4 dorsal root tracing (A), higher magnification of the boxed area in A (B).

Scale bars: 500 µm in A, 100 µm in B. Arrow: L4 dorsal root.

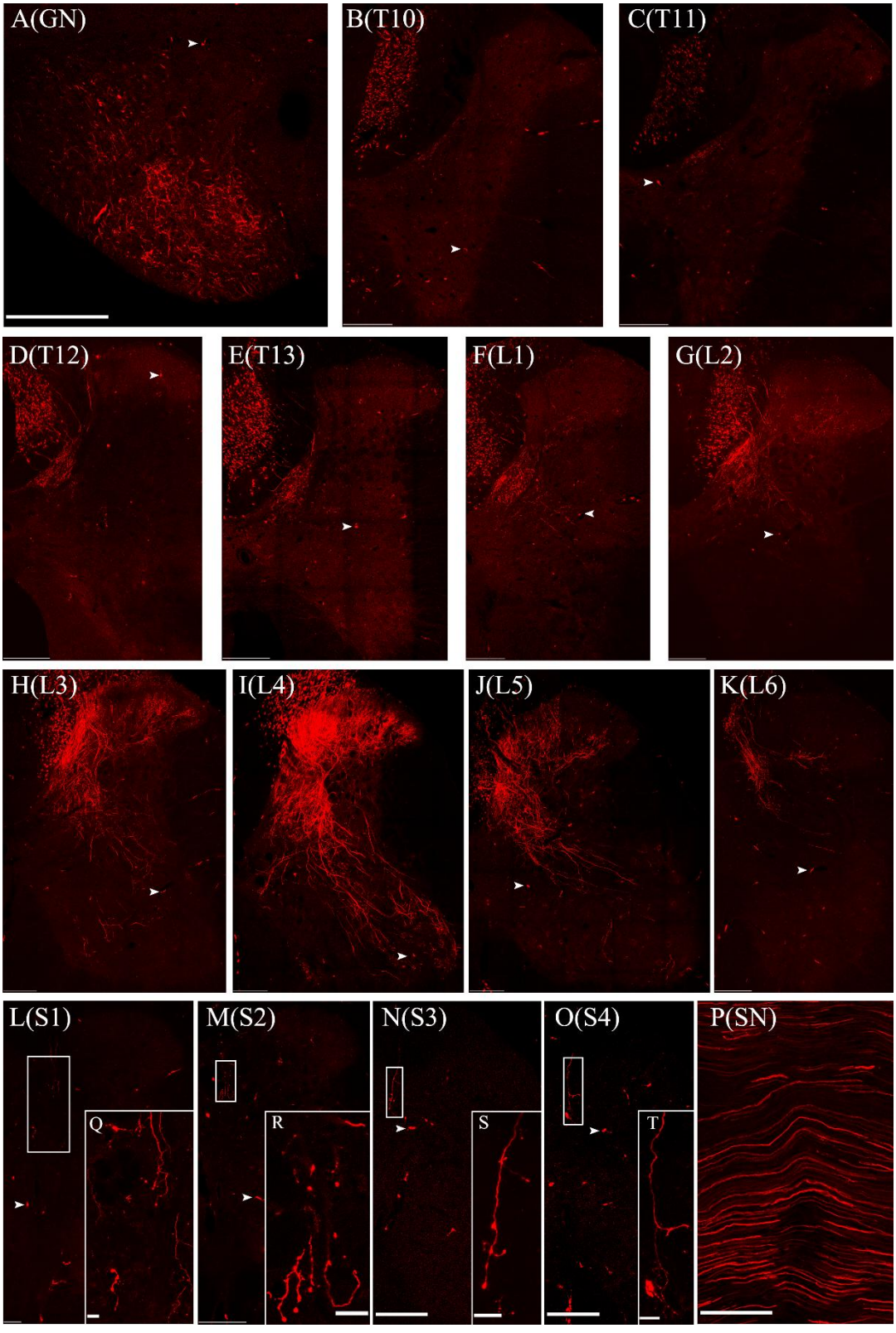

Additional figure 3 Distributions of Texas red-dextran amine in gracile nucleus (A), T10–S4 (B-O) segments of spinal cord and sciatic nerve (P) after L4 DR tracing. Higher magnification of the boxed areas in L–O (Q–T).

Scale bars: 200 μm in A–P, 25 μm in Q–T. Arrowheads: Pericytes; GN: gracile nucleus; SN: sciatic nerve